



Ultrasound-assisted handling force reduction during the solar silicon wafers production



S. Saffar^a, A. Abdullah^b, S. Gouttebroze^c, Z.L. Zhang^{a,*}

^a Department of Structural Engineering, Norwegian University of Science and Technology, NO-7491 Trondheim, Norway

^b Mechanical Engineering Faculty, Amirkabir University of Technology, 424, Hafez Avenue, Tehran, Iran

^c SINTEF Materials and Chemistry, NO-0314 Oslo, Norway

ARTICLE INFO

Article history:

Received 23 April 2013

Received in revised form 29 November 2013

Accepted 19 December 2013

Available online 4 January 2014

Keywords:

Friction reduction

Handling

Silicon wafer

Ultrasonic transducer

ABSTRACT

Surface adhesion between wet wafers poses great challenges for silicon wafer handling. It has been shown that both the shear and normal handling forces of the solar silicon wafers can be dramatically reduced by using the ultrasound energy. Approximately 20 and 5 times reduction in horizontal and vertical forces were achieved by as low power as 10 W, and a good agreement was found between the measured values and the predictions of a simple model for the effect of longitudinal vibration we developed.

© 2013 Elsevier B.V. All rights reserved.

1. Introduction

Currently more than 80% of all commercial solar cells are made of silicon [1]. The need to increase the efficiency and lower the cost of silicon wafers promotes the use of thinner and larger wafers [2]. However, recent industrial studies have shown that the use of thinner wafers can lead to unacceptable yields arising from wafer and cell breakage due to handling, transport and/or processing during solar cell production [3,4]. Since about 40–60% of the total cost is due to fabrication of the silicon wafer, safe handling is an important issue [5].

Suction process is the most common (and critical step for breakage) process in the handling of silicon wafers. It is very desirable for industry due to the breakage reduction of silicon wafers if suction force is reduced somehow. The vacuum pressure of suction cups (suction force) is proportional to the adhesion force between wet wafer (due to wafer singulation) and support. Therefore, reduction in adhesion force could be interesting to be concentrated on. Vibration can be a good candidate to reduce the adhesion force. In fact, static friction coefficient converts to the dynamic friction coefficient which is much smaller than static one.

Friction process with vibration is an important phenomenon because the influence of vibration can cause significant change in the friction process. Some studies [6–16] have found that vibration can reduce friction. It has been shown that both mean friction force and wear rate increase or decrease depending on the vibration

parameters [17,18]. Several studies [19–23] observed that the reduction of friction force depends on roughness of the rubbing surfaces, relative motion, type of material, temperature, normal force, stick slip, relative humidity, lubrication and vibration. Among these factors normal load and sliding velocity are the two major factors that determine the variation of friction [24]. It was reported [25–28] that friction coefficient of metals and alloys varies under different operating conditions. Other studies have found that vibration can reduce wear (reduction in friction). They have shown that micro-vibrations (10–100 μm amplitude) can reduce sliding wear up to 50% [29–37]. Recently, high power ultrasound (frequency up to 100 kHz and high amplitude 100 μm) have been used to control friction in metal working [38–43], wire drawing [44–47], and cutting [48–50].

The sticking force between contacting wet surfaces can be manipulated by ultrasound. However, this technique of silicon wafer handling has not yet been investigated. Hence, the main contribution of this paper is the development of a safe handling methodology by using ultrasound energy. A simple analytical model is proposed to show that using ultrasound can reduce the sticking force. Experiments are also performed to verify the proposed approach. The results of the theoretical investigations and the experiments show good agreement.

2. Theory

Friction issue falls into two categories: contact scenario and friction mechanisms. The first category of friction issue consists of the asperity interaction scenario itself. This scenario only

* Corresponding author. Tel.: +47 735 92530; fax: +47 735 94701.

E-mail address: zhiliang.zhang@ntnu.no (Z.L. Zhang).

considers the normal distance between asperities of both surfaces as a function of the relative horizontal translation between them. The second category discusses the mechanisms governing friction: creep, adhesion and geometrical deformation of asperities.

2.1. Contact scenario

On the microscopic level, smooth surfaces seem “rough.” The surface topography plays an important role in surface interactions. When these surfaces are pressed against each other, the true contact area usually is from 1/400 to 1/10,000 of the apparent area observed by the naked eye. The protuberant features are called asperities. One of the oldest and simplest micro-contact models is the Greenwood–Williamson model [51], which assumed that surfaces were composed of hemi-spherically tipped asperities. The asperities assume by a uniform sphere and a symmetrical Gaussian distribution of asperity heights. The Hertz equations governing elastic contact of spheres and half spaces are utilized to calculate the load, contact area, and contact pressure acting on a deformed asperity.

The contact scenario is illustrated schematically in Fig. 1. Fig. 1A shows two rough objects in contact together, at their surfaces, while the dashed line presents the upper object translated horizontally to the left over a certain distance. As a result, some asperity contacts will persist (a and d), some will disappear (b and e) and new ones will occur (c). The normal distance between the two contacting surfaces can also be transformed to one flat surface and one rough surface (Fig. 1B). Fig. 1C shows the equivalent asperity, of contact point a, for four different time instances of its lifecycle. An overlap between the two surfaces corresponds to a contact between the two asperities [52].

Asperities of the surface increases by using external high frequency vibration and the real contact area reduces between vibrating surfaces [53–55]. In fact, vibration amplitude adds to the existence asperities at the interface. Also, Velocity-weakening of kinetic friction akin to the Stribeck effect in lubricated contacts,

is the phenomenon of decreasing friction force with increasing sliding velocities, (or, in more simplified treatments, the assumption that kinetic friction be lower than static friction, both values being assumed constant). Hence, the friction force tends to be reduced under external high frequency vibration.

2.2. Friction mechanisms

2.2.1. Formulation of the model-contact scenario with the friction mechanisms

The contact surfaces of two blocks rubbing against each other (see Fig. 2A) can be represented by a flexible surface containing all the possible equivalent asperity contacts, each with its own equivalent stiffness, mass and shape depending on the characteristics of the two corresponding interlocking asperities. Each possible equivalent asperity contact has its own individual rigid, shaped lower surface. Fig. 2B shows the life cycle of one such equivalent asperity, where it is assumed that the upper surface is moving from left to right with respect to the fixed lower surface. Topographical characteristics are assigned to both surfaces. The equivalent characteristics of the two interacting asperities (namely stiffness, mass, compression and adhesion) are lumped into one point (●), for simplicity of treatment. This point (Fig. 2B) is initially moving freely (i), until it touches the lower rigid surface (ii), after sticking to and then slipping over the lower profile it breaks completely loose from the lower profile (iii). In case (ii) the asperity is called to be in an active state, for the other cases the asperity is called to be inactive. (This may be reminiscent of the Tomlinson–Prandtl atomic model, except that it accounts for creep, adhesion and load-carrying, which prove essential in revealing friction force dynamics). In this case, we have ignored the possible vibrations of a contacting asperity.

From the moment the asperity becomes active, it will begin to follow the profile of the lower surface, by deforming normally ς and tangentially ξ , resulting in a normal and tangential force. The normal force, $F_n(t)$, is given by $k_n \varsigma(t) f(\xi)$, where k_n is the normal

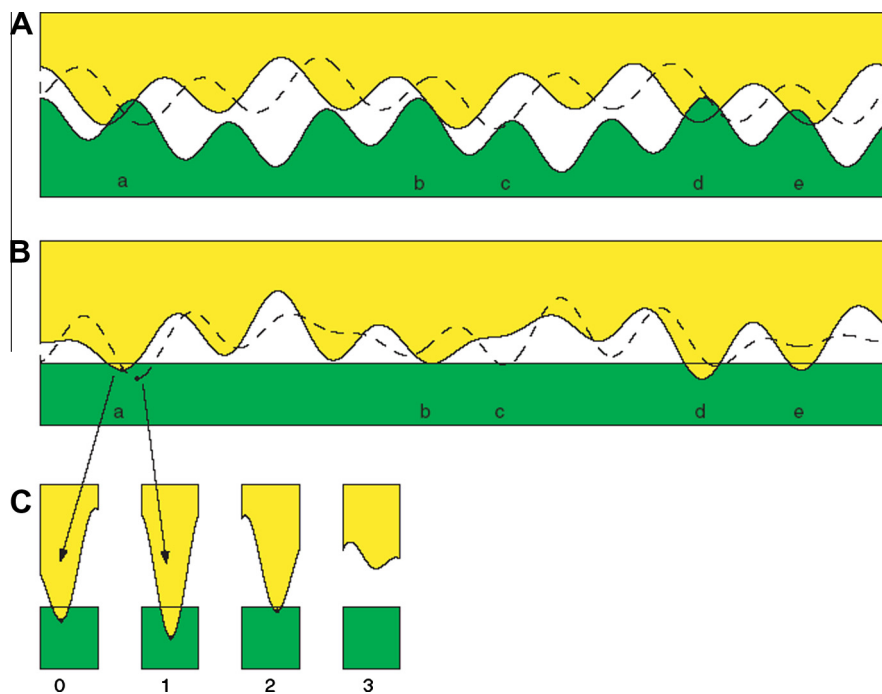


Fig. 1. A schematic representation of friction mechanism. The upper figure shows two surfaces in sliding contact with each other. The dotted line corresponds to the upper surface shifted to the right over a certain distance. The middle figure shows the transformation of the upper figure where the lower surface becomes a flat surface (note the different shape for the shifted surface). The lower figure shows the transformed surfaces of point a for four different shift values. The first and the second one correspond to the full and dotted lines in the middle figure [52].

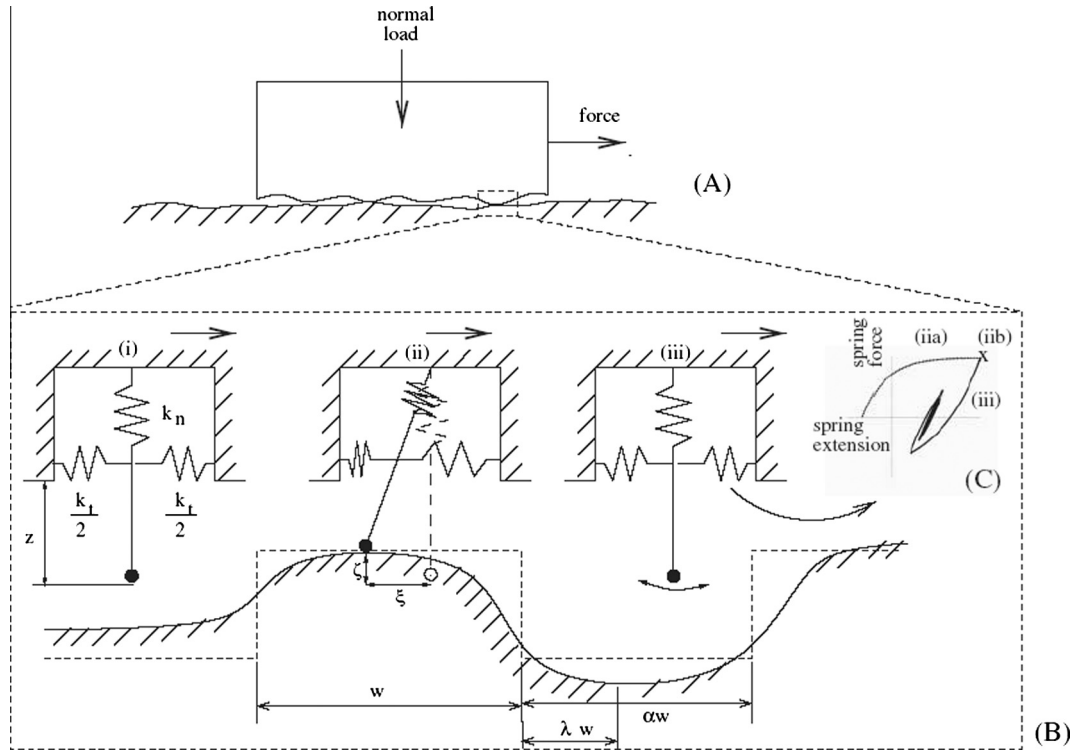


Fig. 2. Figure A shows a general contact between two objects. Figure B shows the life cycle of one asperity contact: (i) no contact, (ii) contact, (iii) loss of contact. Figure C shows the spring force behavior as a function of the spring extension during a life cycle of an asperity contact: (ii a)—during stick, (ii b) x during slip, and (iii) when losing contact [52].

stiffness and $f \leq 1$ is a weighting function, and the tangential force is given by $F(t) = k_t \xi(t)$ where k_t is the tangential stiffness. The maximum tangential force an asperity can sustain, before slipping, equals the adhesion force: $F_{\mu}(t) = \mu(t) \cdot k_n \cdot \zeta(t)$. Here, the expedient local friction coefficient $\mu(t)$ is function of the contact time, owing to normal creep. This behavior can be deduced from the static friction versus dwell-time relation [52].

Coulomb in 1785 [56] was probably the first to explore this time dependence; he reported a power-law increase of static friction with time of contact. As a rule, static friction F_s grows with dwell time. An overview of the various formulae for such dependence, as found or postulated by various authors, is given by Gitis and Volpe [57]. While any appropriate relation may be used according to the situation at hand, it has chosen exponential saturation for simplicity of interpretation:

$$\mu(t) = \mu_0 + (\mu_{\infty} - \mu_0) \cdot \left(1 - \exp\left(1 - \frac{t - t_0}{\tau_{\mu}}\right)\right) \quad (1)$$

with t_0 the time instance when contact occurs, μ_0 and μ_{∞} the local friction coefficients at initial and infinite contact time, and τ_{μ} a characteristic creep time constant. (Note that not all postulated formulae lead to saturation of the friction force in time, but they all lead to saturation in the rate of increase.) Thus, depending on the relative values of μ , k_n , k_t and the relative topography, the asperity tip (•) will initially “stick” to the lower profile then slip on the profile and, finally, break completely loose from the profile.

It is obvious that once ultrasonic applied to the asperities $\mu(t)$ tends to reduce to μ_0 . Since ultrasonic vibration does not permit to the asperities to stick to each other and also eliminate the creep effect ($\mu_{\infty} = \mu_0$). Therefore, the adhesion force reduces by using ultrasonic vibration.

2.2.2. Friction coefficient reduction by using external friction

There are theories based on resonance between the natural frequency of the contact area and the external vibration frequency

that explain the decrease in the friction coefficient because of conversion of static friction coefficient to the dynamic friction coefficient. Here, we propose a simple mass-spring-damping model for longitudinal vibration induced adhesion force reduction. The equilibrium of forces acting at a contact interface between sticking asperities is described in Fig. 3. The coefficient of friction is given by

$$\mu(\chi, t) = \frac{F_T}{F_N + mg} \chi \quad (2)$$

where F_T and F_N are the tension and normal forces, respectively. The friction coefficient μ is influenced by χ , which is a term describing the quality of the surfaces. The relative static friction, μ_{rel} , is defined as the ratio of the static friction coefficient measured in the case with vibrational assistance over the static friction coefficient measured without vibration assistance.

$$\mu_{rel} = \frac{\mu_{ext vib}}{\mu_{no vib}} \quad (3)$$

A static friction coefficient under the influence of an external vibration can then be described as follows if Eq. (2) is used:

$$\mu_{ext vib} = \frac{\ddot{x} + 2\psi\omega_0\dot{x} + \omega_0^2x}{F_N/m + g} \quad (4)$$

where $\omega_0 = (k/m)$ is natural angular frequency, $\psi = C/2(km)^{1/2}$ is damping coefficient and $\chi = 1$. With harmonic oscillation (ω), the relative position between the materials varies according to $x = A \sin(\omega t)$. Inserting into Eq. (4), the results

$$\mu_{ext vib} = \frac{A\omega_0^2}{F_N/m + g} \left[\left(1 - \left(\frac{\omega}{\omega_0}\right)^2\right)^2 + \left(\frac{2\psi\omega}{\omega_0}\right)^2 \right]^{1/2} \sin(\omega t + \phi) \quad (5)$$

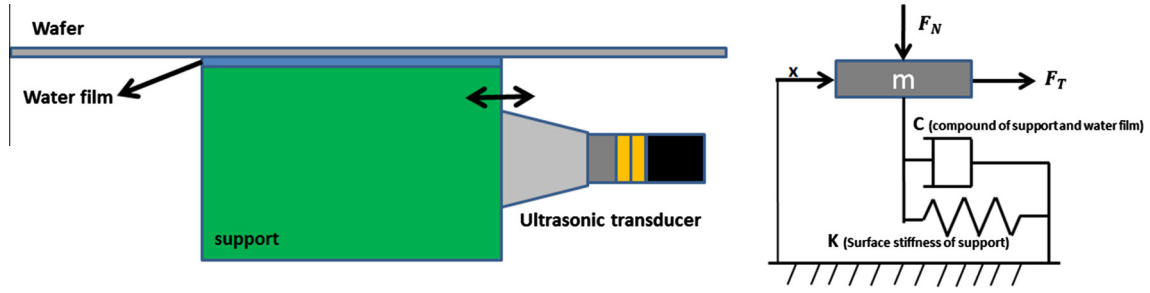


Fig. 3. Model of the friction surface with grip.

The Φ can be written as:

$$\phi = \arcsin \left(\frac{2\psi\omega/\omega_0}{\left\{ \left[1 - (\omega/\omega_0)^2 \right]^2 + (2\psi\omega/\omega_0)^2 \right\}^{1/2}} \right) \quad (6)$$

For low frequency, the mass and damping forces are negligible, which leads to the following correlation:

$$\mu_{novib} = \frac{A\omega_0^2}{F_N/m + g} \sin(\omega t) \quad (7)$$

By inserting Eqs. (5) and (7) into (3), the ratio of relative static friction coefficient can be obtained as follows:

$$\mu_{rel} = \left[\left(1 - \left(\frac{\omega}{\omega_0} \right)^2 \right)^2 + \left(\frac{2\psi\omega}{\omega_0} \right)^2 \right]^{1/2} \frac{\sin(\omega t + \Phi)}{\sin(\omega t)} \quad (8)$$

The above equation can be simplified to

$$\mu_{rel} = \left[\left(1 - \left(\frac{\omega}{\omega_0} \right)^2 \right)^2 + \left(\frac{2\psi\omega}{\omega_0} \right)^2 \right]^{1/2} \quad (9)$$

The variation of adhesion force as a function of vibration frequency and different damping coefficient is plotted in Fig. 4. The angular natural frequency, ω_0 , was set to 20 kHz, which is the common frequency used in industrial high power ultrasonic applications. As shown in Fig. 4, μ_{rel} reduces dramatically if it is exited at the natural frequency of the system (20 kHz).

The presence of liquid films of the capillary condensates or pre-existing films of liquid can powerfully enhance the adhesion between solid bodies [58–61]. Liquid-mediated adhesive forces can be divided into two components: a meniscus force due to surface

tension and a rate-dependent viscous force. These forces increase for smaller gaps and smoother surfaces.

For an applied normal force which is less than the meniscus force there is no tendency to separate the surfaces. The total separation load W (adhesion force F_{ad}) is the summation of the meniscus force (F_m) and the viscous component in the normal direction (F_{vn}): $W = F_{ad} = F_m + F_{vn}$.

The meniscus force due to the Laplace pressure is given by [62]:

$$F_m = \int \int_{\Omega} p_L(x, y) d\Omega = \gamma_1 \int \int_{\Omega} \frac{1}{r_1} d\Omega \approx \gamma_1 (\cos\theta_1 + \cos\theta_2) \frac{\Omega}{\bar{s}} \quad (10)$$

where p_L is the Laplace pressure, r_1 is the meniscus radius, \bar{s} is the mean meniscus height, and Ω is the projected area of meniscus envelope which intersects the upper contacting asperity at a mean meniscus height. For the case of two flat surfaces separated by a liquid film of thickness h , and for projected area of the meniscus A_m comprising the liquid film, F_m is [58,59].

$$F_m \approx \frac{A_m \gamma_l (\cos\theta_1 + \cos\theta_2)}{h} \quad (11)$$

Comparison Eqs. (10) and (11) demonstrates that Ω is always smaller than A_m . Also, \bar{s} and h might be equal. It is obvious from Eq. (10) that F_m is proportional to the contact area, A_m , and the contact area reduces during vibration. Since, the roughness of the vibrating support surface increases due to wave propagation. Hence, the support surface in vibration state can be assumed rougher than the case without vibration. The F_m^{vib} is considered instead of F_m when vibration is employed. Then, the F_m^{vib} is smaller than F_m because of the reduction in A_m during vibration of support.

The total normal force on the wet interface equals to the externally applied normal force plus the intrinsic meniscus force. Therefore, during sliding, in the absence of any hydrodynamic effects, the force required to initiate or sustain sliding is equal to the

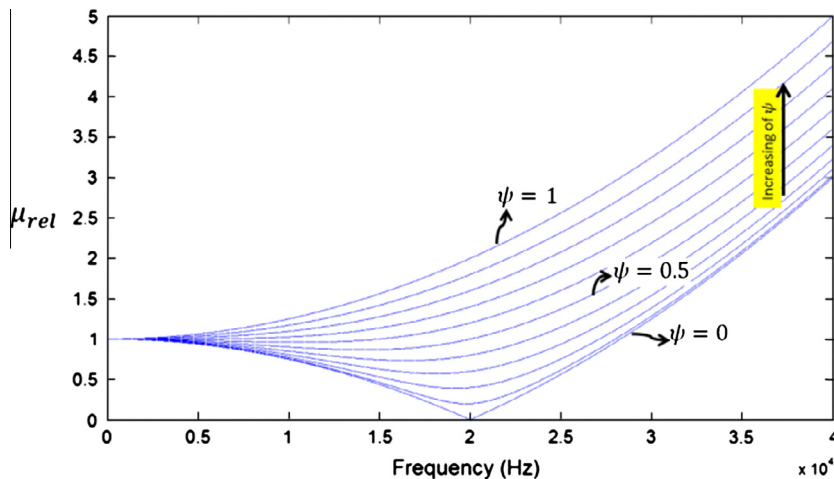


Fig. 4. Effect of longitudinal vibration on (μ_{rel}) in different damping coefficient. Natural frequency of system is 20 kHz.

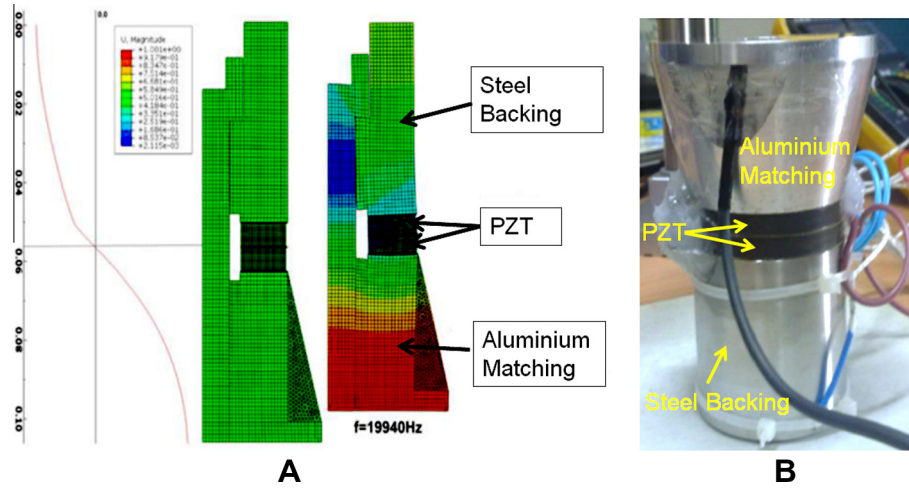


Fig. 5. Transducer layers dimension calculated by ANSYS to have only plane wave (a) finite element model and (b) fabricated transducer.

Table 1

Characteristic of design transducer.

Material	Role	Diameter (mm)		Thickness (mm)	Quantity
		Inner	Outer		
Lead zirconate titanium (PZT)	Vibration source	23	50	6	2
Al 7075-T6	First matching layer	22.6	Smaller Bigger	43	1
Steel 304	Backing	22.6	51	50.6	1
Brass	Connection electrode for 2 PZT	22.8	51	0.5	3
Tapox epoxy	Second matching layer	72	72	0.3	1
Balsa wood	Third matching layer	72	72	6.13	1
High strength steel screw	Mechanical connecting parts	–	–	73.15	1

sum of the intrinsic (true) friction force F_i and the sticking force F_s ; the latter is a combination of the friction force due to the meniscus and viscous effects [63] where μ_r is the true coefficient of friction in the absence of meniscus, and smaller than the measured value of $\mu = F/W$. The sum of W and F_m is the total normal load. The friction force ($\mu_r W$) depends on the material properties and surface topography, whereas F_m depends on the roughness parameters as well as the type of liquid and its film thickness. $\mu_r F_m + F_{viscous}$ is the friction force due to liquid-mediated adhesion, where $F_{viscous}$ is the viscous force in the sliding direction.

The ratio of the normal tensile force \dot{W} required for separation (normally referred to as, F_{ad} , adhesive force) to the normal compressive force W initially applied is often referred to as $\dot{\mu}$ the coefficient of adhesion [58,59].

The coefficient of friction, μ , including the effect of the meniscus and viscous force, and the adhesion coefficient, $\dot{\mu}$, are given by

$$\mu = \frac{F}{W} = \mu_r \left(1 + \frac{F_m}{W} \right) + \frac{F_{viscous}}{W} \quad (12a)$$

$$\dot{\mu} = \frac{\dot{W}}{W} = \frac{F_{ad}}{W} \quad (12b)$$

In our model the effect of the $F_{viscous}$ is included by using damping C , therefore, the Eq. (12) simplified to

$$\mu = \frac{F}{W} = \mu_r \left(1 + \frac{F_m}{W} \right) \quad (13a)$$

$$\dot{\mu} = \frac{\dot{W}}{W} = \frac{F_m}{W} \quad (13b)$$

The Eq. (13) is rewritten by considering the μ_{rel} definition as follows:

$$\mu_{rel} = \mu_{rel} \frac{\left(1 + \frac{F_m^{vib}}{W} \right)}{\left(1 + \frac{F_m}{W} \right)} \quad (14a)$$

$$\dot{\mu}_{rel} = \frac{F_m^{vib}}{W} \quad (14b)$$

As previously discussed, F_m^{vib} is smaller than F_m in Eq. (14) $F_m^{vib} < F_m$. Also, based on Fig. 4 the μ_{rel} can be reduced if the system excited at its natural frequency. Therefore, both μ_{rel} and $\dot{\mu}_{rel}$ can be reduced by using ultrasound at resonance condition.

By assuming $\psi = 0.05$ the μ_{rel} reduces to 0.065 (15.38 times) at frequency of 20 kHz. Therefore, Eq. (14) predicts that the sliding force can be reduced at least 15.38 times by using ultrasound.

3. Experimental setup

In order to verify the approach, an experimental study was carried out. An ultrasonic transducer was designed and fabricated to generate the longitudinal ultrasound power required for the tests (Fig. 5 and Table 1). To design a transducer for plane wave propagation only, it is sufficient to model the energy source for the PZT and matching layers by adding a backing layer in the ANSYS software such that the longitudinal resonance frequency can be found by changing the backing, PZT and the matching layer(s) (especially the matching layers which are closer to the PZT side) thicknesses. For instance, Fig. 5(a) shows the PZT transducer designed using the finite element method (FEM) for 4-layer experiments after calculation of the matching layers to produce pure plane wave generation. The transducer manufactured according to the FEM results is shown in Fig. 5(b) and Table 1.

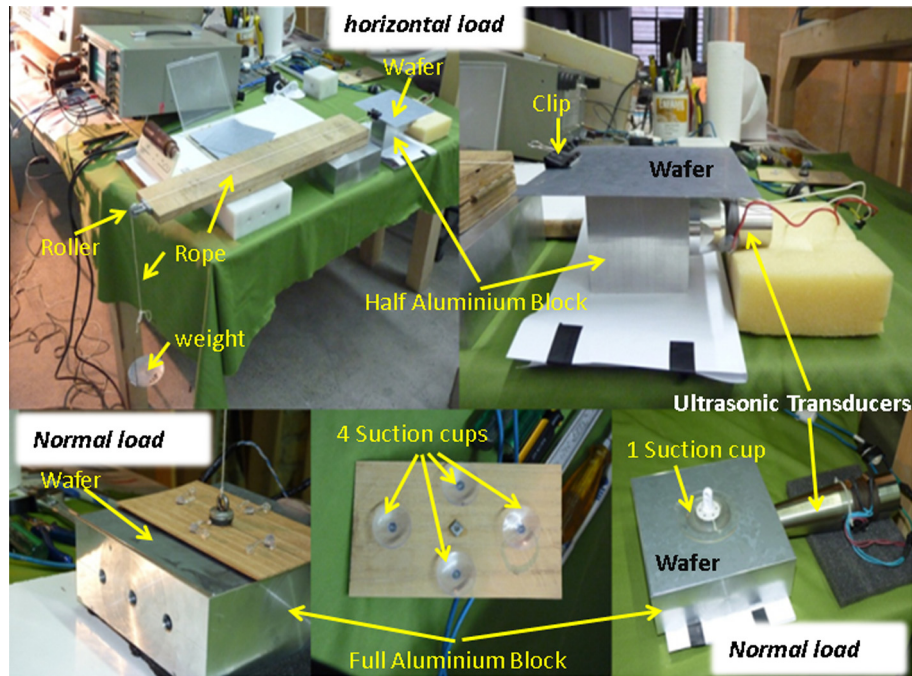


Fig. 6. The employed equipment for experimental test (Aluminum block as support of wafer).

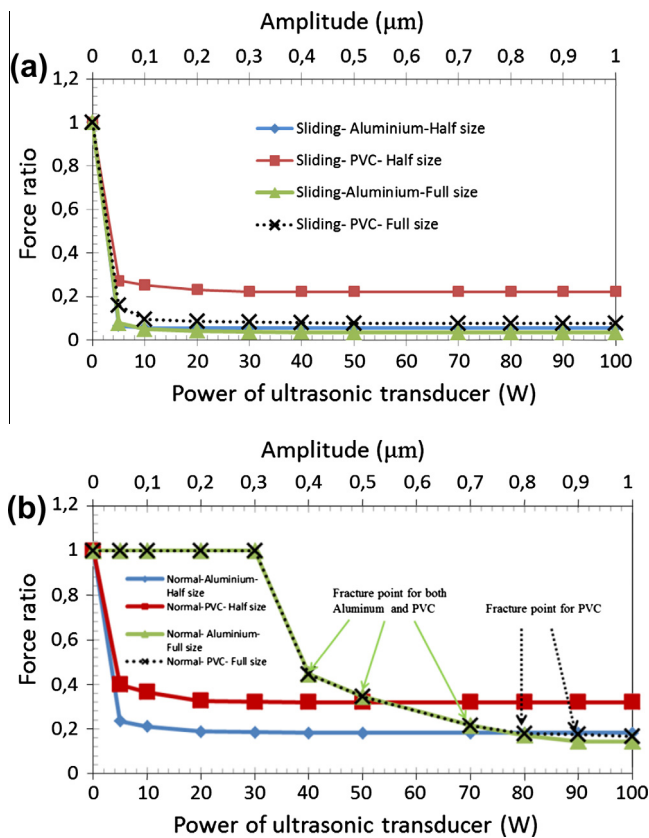


Fig. 7. The effect of ultrasonic power on (a) sliding and (b) normal wafer handling.

The resonance frequency of 20 kHz was chosen as the working frequency. The unit must operate at the resonance condition, and therefore, an electrical matching unit is used to match the electrical circuit and ensure that the transducer always remains in the

resonance condition. The ultrasonic generator driving the transducer could be adjusted to produce vibration amplitudes (peak-to-peak) at the contact region between zero and 20. Also, an adjustable power supply has been employed to set the ultrasonic power in powers which are appropriate for the tests. Multi-crystalline silicon wafers ($156 \times 156 \times 0.18 \text{ mm}^3$) and average surface roughness of 466.73 nm produced by REC (wafer and solar module manufacturer in Porsgrun, Norway) are used as sample of tests. As support of wafers, PVC (PVC Type I Grade I and average roughness of 1.6 μm) and Aluminum (1100 series) blocks (fabricated by milling with average roughness of 1 μm) with two different sizes, $160 \times 160 \text{ mm}^2$ and $80 \times 80 \text{ mm}^2$ which are called *full* and *half* size respectively were attached to an ultrasonic transducer. The tests have been done in two wafer picking configurations, horizontally and normally. The separation loads of wafer from the support surface are measured by a simple system (roller, rope and weights) with and without presence of the ultrasound (see Fig. 6). As shown in Fig. 6, the vertical tests have been measured by employing two types of suction cup, 1 large (diameter of 60 mm) and 4 small (diameter of 20 mm). The results from one suction cup are presented due to the similarity of the results between 1 and 4 suction cups. The experiments were conducted by varying incrementally both the horizontal and normal load by using the weights (the resolution of weight measuring is 0.05 N to reach the moment of slip or separation of the wet wafer from the support surface. The surface of the supports is wetted by water and using a blade to uniform the thickness of water film. The separation load is measured in different amplitudes of vibration. All experiments were carried out at 20°C . Five measurements were made for each set of conditions, and the data points reported represent the mean, standard deviation and total range of the sticking force.

4. Results and discussion

As shown in Fig. 7(a) and Table 2, by power of 10 W , the sliding force decreases approximately 19 times when the half size Aluminium block was used. The sliding force reduces 4 times for a half

Table 2

Average sliding force in different ultrasonic transducer power.

Average sliding force (N)		Half size				Full size			
Transducer parameters		Aluminum		PVC		Aluminum		PVC	
Amplitude (μm)	Power (W)	Av_m^a	STD ^a	Av_m^a	STD ^a	Av_m^a	STD ^a	Av_m^a	STD ^a
0	0	4.65	0.0791	4.95	0.079	25	0	25	0
0.05	5	0.3		1.35		1.95		3.95	0.0707
0.1	10	0.25		1.25		1.25		2.35	
0.2	20	0.25	0	1.15	0.0354	1.05	0.0354	2.15	0.0354
0.3	30	0.25		1.1		0.95		2.05	
0.4	40	0.25		1.1		0.9		2	
0.5	50	0.25		1.1		0.85		1.95	
0.7	70	0.25		1.1		0.85		1.95	
0.8	80	0.25		1.1		0.85		1.95	
0.9	90	0.25		1.1		0.85		1.95	
1	100	0.25		1.1		0.85		1.95	

^a STD: Standard Deviation and Av_m = Average load.**Table 3**

Average normal force in different ultrasonic transducer power.

Average normal force (N)		Half size				Full size			
Transducer parameters		Aluminum		PVC		Aluminum		PVC	
Amplitude (μm)	Power	Av_m^a	STD ^a	Av_m^a	STD ^a	Av_m^a	STD ^a	Av_m^a	STD ^a
0	0	8.65	0.0316	8.85	0.0707	50		50	
0.05	5	2.03	0.0245	3.53	0.0245	50		50	
0.1	10	1.83		3.23		50	0	50	0
0.2	20	1.63		2.88		50		50	
0.3	30	1.6	0.047	2.84	0.0374	50		50	
0.4	40	1.58		2.83		Wafer failure		Wafer failure	
						22.25	0	22.25	0
0.5	50	1.58		2.83		Wafer failure		Wafer failure	
						17.25	0	17.25	0
0.7	70	1.58		2.83		Wafer failure		Wafer failure	
						10.75	0	10.75	0
0.8	80	1.58	0.0245	2.83	0.0245	8.55	0.0707	4 failures	
								8.70	0
0.9	90	1.58		2.83		7.25	0.14	3 failures	
								8.40	0.05
1	100	1.58		2.83		7.25	0.0707	8.32	0.0872

^a STD: Standard Deviation and Av_m = Average load.

size PVC block. The maximum reduction (20 times in 10 W and 30 times in 50 W) occurs in aluminum full size block, the corresponding values are approximately, 11 and 13 times for PVC full size block. This discrepancy between Aluminum and PVC blocks is due to the high structural damping capacity of PVC and the acoustic impedance mismatching loss between aluminum matching layer of the transducer and PVC block. Also, Fig. 7(a) showed that power larger than 20 W has no noticeable effect on adhesion force reduction. The similar phenomenon happens after 40 W for full size blocks.

Furthermore, Fig. 7(b) and Table 3 display the ultrasound effect on the vertical separation of wet wafer from the supports. The normal force decreases approximately 4.5 times (10 W power) when the half size aluminum block is used. The similar value is 2.7 times for a half size PVC block. The maximum reduction (7 times at 90 W) occurs in aluminum full size block, while the similar value is approximately, 6 times for PVC full size block at 100 W. Fig. 7(b) also showed that power higher than 30 W has no noticeable effect on force reduction. The similar phenomenon happens after 90 W for full size blocks. It is interesting to note that an unstable situation is observed in Fig. 7(b) and Table 3 for full size blocks. Some wafers were broken in this unstable state which starts from 40 to 70 W for aluminum and 40 to 90 W for PVC support blocks.

Although a partial releasing occurs by using ultrasound, the power is not enough to separate the wafer completely. The wafer tends to be released in the region around the suction cap, but the rest of wafer (corner of wafer) still sticks to the supports. When the power is high enough to separate the whole wafer from the supports, the complete vertical separation occurs again.

The comparison between sliding and vertical handling shows that the capillary force is stronger in vertical handling than horizontal one. The experimental results suggest that the progressively larger sticking force reduction can be obtained by application of low amplitudes (low power) of vibration.

5. Conclusions

In conclusion, a study of the adhesion force between silicon wafer and support surfaces in the presence of ultrasonic vibration has shown that vibration in longitudinal direction can significantly reduce the adhesion force between interacting surfaces. The reduction in sticking force by using ultrasound was greater than 20 times in horizontal and greater than 5 times in vertical wafer handling. The reduction in adhesion force is predicted by a simple analytical model, which agrees well with experimental observations.

Nevertheless these preliminary conclusions should be confirmed using an experimental set-up closer to industrial practice. In addition wafer damage should be evaluated over a large sample set to confirm the potential of this technique.

Acknowledgement

The authors would like thank the NEXTGEN_SI project financed by the REC group and Norwegian Research Council.

References

- [1] H.J. Moller, C. Funke, M. Rinio, S. Scholz, Multicrystalline silicon for solar cells, *J. Thin Solid Films* 487 (2005) 179–187.
- [2] N.G. Dhere, Toward GW/year production of CIGS within the next decade, *J. Sol. Energy Mater. Sol. Cells* 91 (2007) 1376–1382.
- [3] P.S. Dominguez, J.M. Fernandez, Introduction of thinner monocrystalline silicon wafers in an industrial cell-manufacturing facility, in: *Proceedings of the 20th European Photovoltaic Solar Energy Conference*, Barcelona, Spain, 2005.
- [4] P.A. Wang, Industrial challenges for thin wafer manufacturing, in: *Proceedings of the Fourth World Conference on Photovoltaic Energy Conversion*, 1, IEEE, Piscataway, USA, 2006, pp. 1179–1182.
- [5] A.D. Little, H. Scheer, B. Mcnelis, W. Palz, H.A. Ossenbrink, P. Helm, in: *Proceedings of the 16th Europ. Photovolt. Solar Energy Conf.*, James & James Ltd., London, 2000, p. 9.
- [6] D. Godfrey, Vibration Reduces Metal to Metal Contact and Causes an Apparent Reduction in Friction, *ASME Trans.* 1967, pp. 183–192.
- [7] A. Lehtovaara, Influence of vibration on the kinetic friction between plastics and ice, *J. Wear.* 115 (1987) 131–138.
- [8] D.M. Tolstoi, G.A. Borisova, S.E. Grigорова, Friction reduction by perpendicular oscillations, *Sov. Phys. Dokl.* 17 (1973) 907–909.
- [9] O. Wertheim, I. Bucher, On the Influence of Controlled Vibration on Friction, Research Supported by the ISARELI Academy for Science, 2000.
- [10] W. Lenkiewicz, The sliding process—effect of external vibrations, *J. Wear.* 13 (1969) 99–108.
- [11] V. Aronov, A.F. D'souza, S. Kalpakjian, I. Shareef, Interactions among friction, wear, and system stiffness—part 1: effect of normal load and system stiffness, *J. Tribol.* 106 (1984) 54–58.
- [12] V. Aronov, A.F. D'souza, S. Kalpakjian, I. Shareef, Interactions among friction, wear, and system stiffness—part 2: vibrations induced by dry friction, *J. Tribol.* 106 (1984) 59–64.
- [13] V. Aronov, A.F. D'souza, S. Kalpakjian, I. Shareef, Interactions among friction, wear, and system stiffness—part 3: wear model, *J. Tribol.* 106 (1984) 65–69.
- [14] D.H. Hess, A. Soom, Normal vibrations and friction under harmonic loads: part I—hertzian contacts, *J. Tribol.* 113 (1991) 80–86.
- [15] J.W. Lin, M.D. Bryant, Reductions in wear rate of carbon samples sliding against wavy copper surfaces, *J. Tribol.* 118 (1996) 116–124.
- [16] M.T. Bengisu, A. Akay, Stick-slip oscillations: dynamics of friction and surface roughness, *J. Acoust. Soc. Am.* 105 (1999) 194–205.
- [17] T. Skare, J. Stahl, Static and dynamic friction processes under the influence of external vibrations, *J. Wear.* 154 (1992) 177–192.
- [18] K. Kato, A. Iwabuchi, T. Kayaba, The effects of friction-induced vibration on friction and wear, *J. Wear.* 80 (1982) 307–320.
- [19] J.F. Archard, Wear theory and mechanisms, in: *Wear Control Handbook*, ASME, New York, 1980, pp. 35–80.
- [20] D. Tabor, Friction and wear—developments over the last 50 years, Keynote address, in: *Proceedings of the International Conference on Tribology—Friction, Lubrication and Wear*, 50 years on, London, Institute of Mechanical Engineering, 1987, pp. 157–172.
- [21] E.J. Berger, C.M. Krousgrill, F. Sadeghi, Stability of Sliding in a System Excited by a Rough Moving Surface, *ASME*, 1997, pp. 672–680.
- [22] B. Bhushan, *Principle and Applications of Tribology*, Wiley, New York, 1999, pp. 344–430.
- [23] M. Nosonovsky, Model for solid–liquid and solid–solid friction of rough surfaces with adhesion hysteresis, *J. Chem. Phys.* 126 (224701) (2007) 1–6.
- [24] E. Rabinowicz, *Friction and Wear of Materials*, second ed., Wiley, New York, 1995.
- [25] M.A. Chowdhury, M.M. Helali, The effect of relative humidity and roughness on the friction coefficient under horizontal vibration, *Open Mech. Eng. J.* 2 (2008) 128–135.
- [26] M.A. Chowdhury, M.M. Helali, A.B.M. Toufique, The frictional behavior of mild steel under horizontal vibration, *Tribol. Int.* 42 (2009) 946–950.
- [27] M.A. Chowdhury, S.M.I. Karim, M.L. Ali, The influence of natural frequency of the experimental set-up on the friction coefficient of copper, *J. Eng. Tribol.* 224 (2009) 293–298.
- [28] M.A. Chowdhury, D.M. Nuruzzaman, M.L. Rahaman, Influence of external horizontal vibration on the coefficient of friction of aluminium sliding against stainless steel, *J. Ind. Lubr. Tribol.* 63 (2011) 152–157.
- [29] M.D. Bryant, J.W. Lin, Photoelastic visualization of contact phenomena between real tribological surface, with and without sliding, *J. Wear.* 170 (1993) 267–279.
- [30] M.D. Bryant, J.W. Lin, Reduction of wear rate and contact interface observations for carbon samples sliding against wavy and smooth copper surfaces, in: *Proceedings, Effects of Mechanical Stiffness and Vibration on Wear*, ASTM STP 1247, American Society for Testing and Materials, Philadelphia, PA, 1995, pp. 32–45.
- [31] M.D. Bryant, J.W. Lin, Methods and Apparatus to Reduce Wear on Sliding Surfaces, U.S. Patent 5,466,979, issued November 14, 1995 to UT-Austin, 1995.
- [32] M.D. Bryant, A. Tewari, J.W. Lin, Wear rate reductions in carbon samples conducting current and sliding against wavy copper surfaces, *J. IEEE Trans. Compon., Hybrids Manuf. Technol.-Part A* 18 (1995) 375–381.
- [33] M.D. Bryant, A. Tewari, D. York, Effects of micro (rocking) vibrations and surface waviness on wear and wear debris, *J. Wear.* 216 (1998) 60–69.
- [34] M.D. Bryant, D. York, Measurements and correlations of slider vibrations and wear, *J. Tribol.* 122 (2000) 374–380.
- [35] T. Moriwaki, E. Shamoto, Ultra precision diamond turning of stainless steel by applying ultrasonic vibration, *J. CIRP Ann.-Manuf. Technol.* 40 (1991) 559–582.
- [36] H. Weber, J. Herberger, R. Pilz, T.H. Karl-Marx-Stadt, Turning of machinable glass ceramics with an ultrasonically vibrated tool, *J. CIRP Ann.-Manuf. Technol.* 33 (1984) 85–87.
- [37] A.C. Tam, B. Bhushan, Reduction of friction between a tape and a smooth surface by acoustic excitation, *J. Appl. Phys.* 61 (1987) 1646.
- [38] A. Siddiq, T. El Sayed, Ultrasonic-assisted manufacturing processes: variational model and numerical simulations, *Ultrasonics* 52 (2012) 521–529.
- [39] J.C. Hung, C. Hung, The influence of ultrasonic-vibration on hot upsetting of aluminum alloy, *Ultrasonics* 43 (2005) 692–698.
- [40] Y. Ashida, H. Aoyama, Press forming using ultrasonic vibration, *J. Mater. Process. Technol.* 187–188 (2007) 118–122.
- [41] T. Oiwa, Friction control using ultrasonic oscillation for rolling-element linear-motion guide, *Rev. Sci. Instrum.* 77 (2006) 1–4. 016107.
- [42] M. Rosochowska, A. Rosochowski, FE simulation of ultrasonic back extrusion, *AIP Conf. Proc.* 907 (2007) 564–569.
- [43] Kh. Armaghan, G.A. Christophe, A. Gabriel, B. Régis, Effects of vibrations on metal forming process: analytical approach and finite element simulations, *AIP Conf. Proc.* 1315 (2010) 787–792.
- [44] Y. Jiang, X. Tao, Investigations on the Effects of Ultrasonic Vibrations in the Wire Drawing, in: *IEEE International Ultrasonics Symposium Proceedings*, 2008, pp. 2134–2137.
- [45] B.N. Mordiyuk, V.S. Mordiyuk, V.V. Buryak, Ultrasonic drawing of tungsten wire for incandescent lamps production, *Ultrasonics* 42 (2004) 109–111.
- [46] A. Shah, H. Gaul, M. Schneider-Ramelow, H. Reichl, M. Mayer, Y. Zhou, Ultrasonic friction power during Al wire wedge–wedge bonding, *J. Appl. Phys.* 106 (013503) (2009) 1–8.
- [47] T. Jimma, Y. Kasuga, N. Iwaki, O. Miyazawa, E. Mori, K. Ito, H. Hatano, An application of ultrasonic vibration to the deep drawing process, *J. Mater. Process. Technol.* 80–81 (1998) 406.
- [48] Y. Schneider, S. Zahn, C. Schindler, H. Rohm, Ultrasonic excitation affects friction interactions between food materials and cutting tools, *Ultrasonics* 49 (2009) 588–593.
- [49] K. Iin Kuo, Ch. Chen, Rotary ultrasonic-assisted milling of brittle materials, *Trans. Nonferr. Metal. Soc. China* 22 (2012) 793–800.
- [50] M.J. Nategh, H. Razavi, A. Abdullah, Analytical modeling and experimental investigation of ultrasonic-vibration assisted oblique turning, part I: Kinematics analysis, *Int. J. Mech. Sci.* 63 (2012) 1–11.
- [51] J.A. Greenwood, J.B.P. Williamson, Contact of nominally flat surfaces, *Proc. R Soc. London* (1966) 300–319.
- [52] F. Al-Bender, V. Lampaert, J. Swevers, A novel generic model at asperity level for dry friction force dynamics, *J. Tribol. Lett.* 16 (2004) 81–93.
- [53] B.V. Budanov, V.S. Kuinov, D.M. Tolstoj, Interaction of friction and vibration, *Sov. J. Frict. Wear.* 1 (1980) 79–89.
- [54] L.M. Serdyuk, V.V. Mikityanskii, Reliability of clamping devices of machine tool fixtures with machining system vibrations, *J. Trenie Iznos Mash.* 7 (1986) 266–275.
- [55] F. Dinelli, S.K. Biswas, G.A.D. Briggs, O.V. Kolosov, Ultrasound induced lubricity in microscopic contact, *Appl. Phys. Lett.* 71 (1177) (1997) 1–3.
- [56] D. Dowson, *History of Tribology*, second ed., Professional Engineering London, London, 1998.
- [57] N.V. Gitis, L. Volpe, *J. Phys. D: Appl. Phys.* 25 (1992) 605.
- [58] B. Bhushan, *Principles and Applications of Tribology*, Wiley, New York, 1999.
- [59] B. Bhushan, *Introduction to Tribology*, Wiley, New York, 2002.
- [60] A.W. Adamson, *Physical Chemistry of Surfaces*, fifth ed., Wiley, New York, 1990.
- [61] J.N. Israelachvili, *Intermolecular and Surface Forces*, second ed., Academic, San Diego, 1992.
- [62] X. Tian, B. Bhushan, The micro-meniscus effect of a thin liquid film on the static friction of rough surface contact, *J. Phys. D* 29 (1996) 163–178.
- [63] B. Bhushan, *Tribology, Mechanics of Magnetic Storage Devices*, second ed., Springer, New York, 1996.